The Journal of Chemical Physics

Sequential double ionization of molecules by strong laser fields simulated with time-dependent configuration interaction

Cite as: J. Chem. Phys. **155**, 114103 (2021); https://doi.org/10.1063/5.0060365
Submitted: 17 June 2021 . Accepted: 25 August 2021 . Published Online: 15 September 2021

Paul Hoerner, Wen Li, and H. Bernhard Schlegel

AIP Publishing

The Journal of Chemical Physics ARTICLE scitation.org/journal/jcp

Sequential double ionization of molecules by strong laser fields simulated with time-dependent configuration interaction

Cite as: J. Chem. Phys. 155, 114103 (2021); doi: 10.1063/5.0060365
Submitted: 17 June 2021 • Accepted: 25 August 2021 •
Published Online: 15 September 2021

Paul Hoerner, Wen Li, and H. Bernhard Schlegel[a)]

AFFILIATIONS

Department of Chemistry, Wayne State University, Detroit, Michigan 48202, USA

[a)]Author to whom correspondence should be addressed: hbs@chem.wayne.edu

ABSTRACT

A new time-dependent configuration interaction method has been developed for simulating strong field sequential double ionization of molecular systems. Ionization of the neutral is simulated by time-dependent configuration interaction with single excitations (TD-CIS) and an absorbing boundary. At each time step, the ionized part of the wavefunction from the TD-CIS calculation is transferred to a second time-dependent configuration interaction simulation for ionization of the cation to the dication. The second simulation uses a CISD-IP wavefunction that consists of singly ionized configurations and singly excited, singly ionized configurations (TD-CISD-IP). The transfer between the TD-CIS and TD-CISD-IP simulations is accomplished by partitioning the first ionization rate into contributions from individual orbitals or by singular value decomposition of the absorbed wavefunction. Sequential double ionization simulations have been carried out for HBr in five cycle 800 nm linearly polarized pulses and HI (with spin–orbit coupling) in four cycle 800 nm circularly polarized pulses, with intensities chosen so that the population of the neutral was depleted by the mid-pulse. The singular value decomposition of the cation produced by the first ionization is dominated by a single component for the two orientations considered. The population of the cation rises and then falls as it is ionized to the dication. Depending on the pulse shape and field strength, the ionization of the cation to the dication can continue for several half cycles. For HI with circularly polarized light, the rates for both the first and second ionization peak when the electric field is aligned with the p_π orbital.

I. INTRODUCTION

A strong laser field interacting with atoms and molecules can lead to single, double, and even multiple ionization. In the tunneling regime, with linearly polarized light, electron-recollision-assisted nonsequential double ionization has attracted significant interest in the past due to the role played by the correlated dynamics of electrons.[1–3] In the over-the-barrier ionization regime or with circularly polarized light, sequential ionization dominates.[4] Although perceived as a simpler process, sequential double ionization is important and has been implemented in many experiments to study ionization-initiated electronic dynamics, nuclear dynamics, or the coupling between the two[5–8] either with a single beam or in a two-beam pump–probe setup. This is not without controversy due to the fact that a strong laser field can induce significant dynamics itself when used as a probe and thus requires careful modeling. Furthermore, correlated electron dynamics has been suggested to manifest also in sequential double ionization when the time delay between the first and second ionization was measured.[9–11] Finally, the role of electronic coherence is likely to play an important role in sequential double ionization.[7,11] How to incorporate this effect in the modeling of the dynamics has not been resolved satisfactorily, especially in molecular systems.

Theoretical and computational methods for describing electron dynamics in strong fields have been reviewed recently.[12–16] One and two electron systems can be treated accurately, while approximations such as single active electron (SAE) and strong field approximation (SFA) are often used for many electron atoms and molecules. Time-dependent density functional theory (TDDFT) and time-dependent configuration interaction (TDCI) have been used successfully to simulate strong field, over-the-barrier ionization.

In the present work, we use TDCI with a complex absorption potential to model sequential double ionization. Two TDCI simulations are run in tandem. TDCI with single excitations[17] (TD-CIS) is used for ionization of the neutral to the cation. The ionized part of the wavefunction is transferred coherently and phase matched to a TD-CISD-IP simulation[18] for ionization of the cation to the dication. The cation wavefunction is represented with the CISD-IP approach of Golubeva *et al.*[19] and consists of singly ionized configurations and singly excited, singly ionized configurations. Coupled TD-CIS and TD-CISD-IP simulations are used to describe the sequential double ionization of HBr and HI in ultrashort, intense laser pulses with linear and circular polarization.

II. METHODS

The electronic wavefunction is propagated with the time-dependent Schrödinger equation (atomic units are used throughout the paper),

$$i\hbar\frac{\partial}{\partial t}\Psi(t) = \hat{\mathbf{H}}(t)\Psi(t) = [\hat{\mathbf{H}}_{el} + \hat{\mathbf{V}}^{SOC} - \hat{\vec{\mu}}\cdot\vec{E}(t) - i\hat{\mathbf{V}}^{absorb}]\Psi(t). \tag{1}$$

$\hat{\mathbf{H}}_{el}$ is the field-free non-relativistic electronic Hamiltonian, and $\hat{\mathbf{V}}^{absorb}$ is a complex absorbing potential (CAP). For simulations that include spin–orbit coupling term, the Breit–Pauli spin–orbit coupling operator, $\hat{\mathbf{V}}^{soc}$, is approximated by an effective one electron spin–orbit coupling operator,[20]

$$\hat{\mathbf{V}}^{SOC} = -\frac{\alpha_0^2}{2}\sum_A \frac{Z_A^{eff}}{i}\frac{(\mathbf{r}-\mathbf{r}_A)\times\nabla}{|\mathbf{r}-\mathbf{r}_A|^3}. \tag{2}$$

Simulations of sequential double ionization are carried out by coupling single ionization of a neutral system using TDCI with single excitations (TD-CIS) with ionization of the resulting cation using TDCI with single and double excitation with ionization (TD-CISD-IP). For the TD-CIS simulation involving closed shell systems, the wavefunction includes all $\alpha\rightarrow\alpha$, $\beta\rightarrow\beta$ single excited determinants; for simulations with spin–orbit coupling, $\alpha\rightarrow\beta$, $\beta\rightarrow\alpha$ single excited determinants also need to be included,

$$\Psi_{neutral}(t) = c_0\psi_0 + \sum_{ia} c_i^a\psi_i^a + \sum_{\bar{i}\bar{a}} c_{\bar{i}}^{\bar{a}}\psi_{\bar{i}}^{\bar{a}} + \sum_{i\bar{a}} c_i^{\bar{a}}\psi_i^{\bar{a}} + \sum_{\bar{i}a} c_{\bar{i}}^{a}\psi_{\bar{i}}^{a}. \tag{3}$$

Indices i,j, etc., refer to occupied α molecular orbitals and a,b, etc., refer to unoccupied α molecular orbitals, while $\bar{i},\bar{j}$ and $\bar{a},\bar{b}$ refer to the corresponding β molecular orbitals. The total number of states for TD-CIS is proportional to the number of occupied orbitals times the number of unoccupied orbitals included in the simulation.

TDCI simulations for the cation use the CISD-IP approach of Golubeva *et al.*[19] The time-dependent CISD-IP wavefunction is constructed using the molecular orbitals of the closed shell system and includes singly ionized determinants, ψ_x, and singly excited, singly ionized determinants, ψ_{xi}^a. As in the CIS case, the wavefunction for CISD-IP with spin–orbit coupling needs to include $\alpha\rightarrow\beta$ and $\beta\rightarrow\alpha$ excitations in addition to $\alpha\rightarrow\alpha$ and $\beta\rightarrow\beta$ excitations,

$$\begin{aligned}\Psi_{cation}(t) =& \sum_x c_x\psi_x + \sum_{\bar{x}} c_{\bar{x}}\psi_{\bar{x}} + \sum_{iax} c_{ix}^a\psi_{ix}^a + \sum_{ia\bar{x}} c_{i\bar{x}}^a\psi_{i\bar{x}}^a \\ &+ \sum_{\bar{i}\bar{a}x} c_{\bar{i}x}^{\bar{a}}\psi_{\bar{i}x}^{\bar{a}} + \sum_{\bar{i}a\bar{x}} c_{\bar{i}\bar{x}}^{\bar{a}}\psi_{\bar{i}\bar{x}}^{\bar{a}} + \sum_{i\bar{a}x} c_{i\bar{a}x}^{\bar{a}}\psi_{i\bar{a}x}^{\bar{a}} + \sum_{i\bar{a}\bar{x}} c_{i\bar{a}\bar{x}}^{a}\psi_{i\bar{a}\bar{x}}^{a},\end{aligned} \tag{4}$$

where x and y are the ionized molecular orbitals ($i<x$ when i and x are the same spin). In all subsequent equations, the sums run over all appropriate spin combinations of the orbitals (i.e., over spin-orbitals). The total number of states for TD-CISD-IP is proportional to the number of ionized orbitals times the number of occupied orbitals times the number of unoccupied orbitals included in the simulation.

In simulating sequential double ionization, the norm of cation has to increase at the same rate as the norm of the neutral decreases. Two approaches can be considered for the rate of formation of the cation. The ionization rate for the neutral can be partitioned into contributions from the ionization of individual occupied orbitals. Alternatively, the part of the wavefunction absorbed by the potential can be decomposed into a free electron times a cation wavefunction.

The ionization rate of the neutral can be calculated as the rate of decrease of the norm squared, $\langle\Psi_{neutral}(t)|\Psi_{neutral}(t)\rangle$, which is proportional to the integral over the absorbing potential,

$$\begin{aligned}rate(t) &= -\partial\langle\Psi_{neutral}(t)|\Psi_{neutral}(t)\rangle/\partial t \\ &= \frac{2}{\hbar}\langle\Psi_{neutral}(t)|\mathbf{V}^{absorb}|\Psi_{neutral}(t)\rangle.\end{aligned} \tag{5}$$

For a normalized CIS wavefunction of the neutral, the integral over the absorbing potential is

$$\begin{aligned}&\langle\Psi_{neutral}(t)|\mathbf{V}^{absorb}|\Psi_{neutral}(t)\rangle \\ &= c_0^* c_0\left\langle\psi_0\middle|\mathbf{V}^{absorb}\middle|\psi_0\right\rangle + \sum_{jb} c_0^* c_j^b\left\langle\psi_0\middle|\mathbf{V}^{absorb}\middle|\psi_j^b\right\rangle \\ &\quad + \sum_{ia} c_i^{a\,*} c_0\left\langle\psi_i^a\middle|\mathbf{V}^{absorb}\middle|\psi_0\right\rangle + \sum_{ijab} c_i^{a\,*} c_j^b\left\langle\psi_i^a\middle|\mathbf{V}^{absorb}\middle|\psi_j^b\right\rangle \\ &= \sum_i \mathbf{V}_{ii} + \sum_{ia}\left(c_0^* c_i^a\mathbf{V}_{ia} + c_i^{a*} c_0\mathbf{V}_{ia}\right) \\ &\quad + \sum_{ijab} c_i^{a\,*} c_j^b(\mathbf{V}_{ab}\delta_{ij} - \mathbf{V}_{ij}\delta_{ab}),\end{aligned} \tag{6}$$

where $\mathbf{V}_{pq} = \langle\phi_p|\mathbf{V}^{absorb}|\phi_q\rangle$ are the integrals of the absorbing potential in the molecular orbital basis. The overall ionization rate can be partitioned in contributions from individual occupied orbitals,

$$\begin{aligned}rate(t)_i = \frac{2}{\hbar}\Big[&\mathbf{V}_{ii} + \sum_a\left(c_0^* c_i^a\mathbf{V}_{ia} + c_i^{a\,*} c_0\mathbf{V}_{ia}\right) \\ &+ \sum_{jab} c_i^{a\,*} c_j^b(\mathbf{V}_{ab}\delta_{ij} - \mathbf{V}_{ij}\delta_{ab})\Big].\end{aligned} \tag{7}$$

The rate for ionization for orbital x of the neutral, $rate(t)_x$, is then taken as the rate of increase for the corresponding configuration ψ_x of the cation. The updated coefficients are

$$c_x'(t)\psi_x = (c_x(t) + f(t)\,\phi)\psi_x, \tag{8}$$

where $f(t)$ is chosen so that $c_x'^*(t)\,c_x'(t) = c_x^*(t)\,c_x(t) + rate(t)_x\Delta t$,

$$f(t) = \sqrt{|c_x(t)|^2 + rate(t)_x\Delta t} - |c_x(t)|, \quad \phi = c_x(t)\,/|c_x(t)|, \quad (9)$$

where Δt is the time step and the phase ϕ is chosen to match $c_x(t)$. The updated coefficients $c_x'(t)$ are then propagated to the next time step using the time-dependent Schrödinger equation.

In the second approach, the rate of increase for the singly ionized configurations of the cation is obtained from $\tilde{\Psi}(t)$, the absorbed portion of the wavefunction of the neutral. The normalized absorbed wavefunction is given by

$$\tilde{\Psi}(t) = \mathbf{V}^{absorb}\Psi_{neutral}(t)\,/|\mathbf{V}^{absorb}\Psi_{neutral}(t)| = \sum_{ia}\tilde{c}_i^a(t)\,\psi_i^a$$

where

$$\tilde{c}_i^a(t) = \sum_{jb}\left\langle\psi_i^a\middle|\hat{\mathbf{V}}^{absorb}\middle|\psi_j^b\right\rangle c_j^b(t)\,/|\mathbf{V}^{absorb}\Psi_{neutral}(t)|. \quad (10)$$

If ionization occurs from only one orbital, the absorbed wavefunction can be factored into a wavefunction for the ionized molecule times a wavefunction for the ejected electron,

$$\tilde{\Psi}(t) = \sum_a \tilde{c}_x^a(t)\,\psi_x^a = \tilde{c}_x(t)\,\psi_x \times \sum_a \tilde{c}_a(t)\,\psi^a, \quad (11)$$

where ψ_x is a singly ionized determinant and ψ^a is a single electron in a virtual orbital a (this assumes that the ejected electron is distant enough so that exchange can be neglected).

When ionization can occur from more than one occupied orbital, the coefficients $\tilde{c}_x$ and $\tilde{c}_a$ can be obtained by singular value decomposition (SVD) of $\tilde{c}_x^a$,

$$\tilde{\mathbf{c}} = \tilde{\mathbf{c}}_x\mathbf{w}\,\tilde{\mathbf{c}}_a^T, \quad \tilde{c}_x^a = \sum_{K=1}^{n} w_K\tilde{c}_x^K\tilde{c}_a^K, \quad \sum_K |w_K|^2 = 1, \quad (12)$$

where $\tilde{\mathbf{c}}_x$ and $\tilde{\mathbf{c}}_a$ are unitary matrices and w_K are the weights. Ionizing an electron from more than one orbital leads to a wavefunction that involves several ionized states. Each wavefunction $\tilde{\Psi}^K(t) = \sum_x c_x^K(t)\,\psi_x$ can be a single determinant or a linear combination of determinants corresponding to a coherent superposition of singly ionized configurations.

The occupied, occupied block of the density matrix for the absorbed wavefunction is $\tilde{\rho}_{ij} = \delta_{ij} - \sum_a \tilde{c}_i^{a\,*}\tilde{c}_j^a$. Substituting Eq. (12) into this expression and using the fact that $\tilde{\mathbf{c}}_a$ is a unitary matrix lead to an expression for $\tilde{\rho}_{ij}$ in terms of a superposition of the densities $\tilde{\rho}_{ij}^K$ for the ionized states $\tilde{\Psi}^K$,

$$\begin{aligned}\tilde{\rho}_{ij} &= \delta_{ij} - \sum_a \tilde{c}_i^{a\,*}\tilde{c}_j^a = \delta_{ij} - \sum_a\left(\sum_{K=1}^{n} w_K\tilde{c}_i^K\tilde{c}_a^K\right)^*\left(\sum_{L=1}^{n} w_L\tilde{c}_j^L\tilde{c}_a^L\right)\\ &= \delta_{ij} - \sum_{K,L}^{n} w_K^* w_L\tilde{c}_i^{K\,*}\tilde{c}_j^L\sum_a\tilde{c}_a^{K\,*}\tilde{c}_a^L = \delta_{ij} - \sum_{K,L}^{n} w_K^* w_L\tilde{c}_i^{K\,*}\tilde{c}_j^L\delta_{KL}\\ &= \sum_K^n |w_K|^2\left(\delta_{ij} - \tilde{c}_i^{K\,*}\tilde{c}_j^K\right) = \sum_K^n w_K^2\tilde{\rho}_{ij}^K. \end{aligned} \quad (13)$$

The diagonal elements of the density, $\tilde{\rho}_{ii}$, are the populations of the occupied orbitals of the normalized absorbed wavefunction.

A specific wavefunction K from the first ionization can be propagated further, leading to a second ionization. The weights w_K can be used to partition the total rate into contributions from each $\tilde{\Psi}^K$. The coefficients f_K are chosen so that $\sum_x\left(c_x'^*(t)c_x'(t)\right) = \sum_x\left(c_x^*(t)c_x(t)\right) + |w_K|^2 rate(t)\Delta t$,

$$c_x'(t)\psi_x = \left(c_x(t) + f_K(t)\,\phi\,\tilde{c}_x^K(t)\right)\psi_x, \quad (14)$$

$$\begin{aligned} f_K(t) &= \sqrt{\left|\sum_x c_x^*(t)\,\tilde{c}_x^K(t)\right|^2 + |w_K|^2 rate(t)_x\Delta t} - \left|\sum_x c_x^*(t)\,\tilde{c}_x^K(t)\right|\\ \phi &= \sum_x c_x^*(t)\,\tilde{c}_x^K(t)\Big/\left|\sum_x c_x^*(t)\,\tilde{c}_x^K(t)\right|, \end{aligned} \quad (15)$$

where the phase ϕ is chosen to maximize the overlap between $\tilde{c}_x^K\,\phi$ and c_x.

In practice, the coefficients for the singly ionized determinants, $\tilde{c}_x(t)$, are stored at each time step for the first TD-CIS simulation for the ionization of the neutral. These coefficients are then retrieved in the second TD-CISD-IP simulation for the ionization of the cation. This avoids the need to have two synchronized propagations running simultaneously.

As described in previous papers,[6,17,21–28] the absorbing potential for the molecule is constructed from spherical potentials centered on each atom and is equal to the minimum of the values of the atomic absorbing potentials. The spherical atomic absorbing potential begins at 3.5 times the van der Waals radius of each element (R_H = 9.544 bohrs, R_{Cl} = 13.052 bohrs, R_{Br} = 13.853 bohrs, R_I = 14.882 bohrs), rises quadratically to 5 hartree at approximately R + 14 bohrs, and turns over quadratically to 10 hartree at approximately R + 28 bohrs.

Simulations of strong field ionization were carried out with a linearly polarized five cycle 800 nm (ω = 0.057 a.u.) pulse with a $\sin^2$ envelope,

$$\begin{aligned} E(t) &= E_{\max}\,\sin(\omega\,t/10)^2\,\cos(\omega\,t) \quad \text{for} \quad 0 \le \omega\,t \le 10\pi,\\ E(t) &= 0 \text{ for } \omega t \ge 10\pi, \end{aligned} \quad (16)$$

and a four cycle circular polarized 800 nm pulse in the xz plane with a $\sin^2$ envelope,

$$\begin{aligned} E_x(t) &= E_{\max}\,\sin(\omega t/8)^2[-\cos(\omega t)\cos(\gamma) - \sin(\omega t)\sin(\gamma)],\\ E_z(t) &= E_{\max}\,\sin(\omega t/8)^2[\cos(\omega t)\sin(\gamma) - \sin(\omega t)\cos(\gamma)]\\ &\text{for } 0 \le \omega t \le 8\pi, \quad E_z(t) = E_x(t) = 0 \text{ for } \omega t \ge 8\pi. \end{aligned} \quad (17)$$

E_{max} is the maximum value for the electric field, and γ determines the direction of the field at the maximum of the pulse. The pulse shapes are shown in Fig. 1.

The exponential of the Hamiltonian is used to propagate the time-dependent wavefunction (shown in atomic units, $\hbar$ = 1).

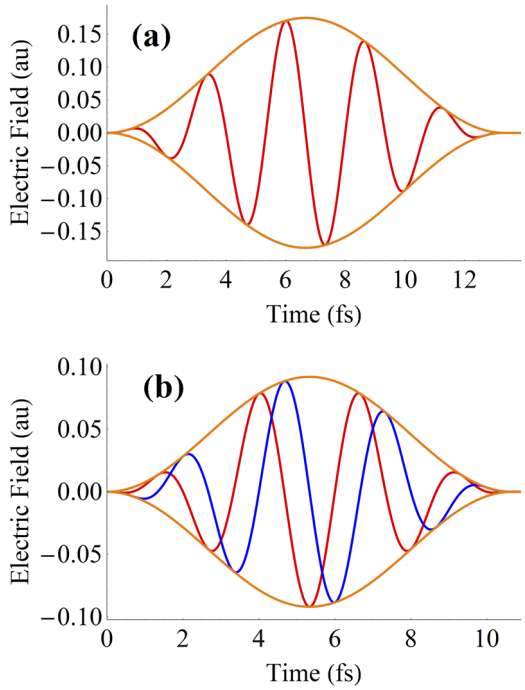

FIG. 1. (a) Five cycle linearly polarized 800 nm pulse with a $\sin^2$ envelope, Eq. (16); (b) four cycle circularly polarized 800 nm pulse with a $\sin^2$ envelope and $\gamma = 0$, Eq. (17); red and blue are the x and z components of the circular pulse propagating in the y direction.

For a linearly polarized pulse, the Trotter factorization of the exponential is

$$\begin{aligned}\Psi(t+\Delta t) &= \exp(-i\hat{\mathbf{H}}\Delta t)\Psi(t),\\ \mathbf{c}(t+\Delta t) &= \exp(-i\,\mathbf{H}_{el}\Delta t/2)\exp(-\mathbf{V}^{absorb}\Delta t/2)\\ &\quad\times \mathbf{W}^{T}\exp(i\,E(t+\Delta t/2)\,\mathbf{d}\,\Delta t)\,\mathbf{W}\\ &\quad\times \exp(-\mathbf{V}^{absorb}\Delta t/2)\exp(-i\,\mathbf{H}_{el}\Delta t/2)\mathbf{c}(t),\end{aligned} \tag{18}$$

where $\mathbf{WDW}^T = \mathbf{d}$ are the eigenvalues and eigenvectors of the transition dipole matrix $\mathbf{D}$ in the field direction. The cost of computing $\exp(-i\mathbf{H}_{el}\Delta t/2)$, $\exp(-\mathbf{V}^{absorb}\Delta t/2)$, $\mathbf{W}$, and $\mathbf{d}$ is proportional to $N_{\text{states}}{}^3$ where N_{states} is the total number of configurations in the simulation. However, these matrices need to be calculated only once at the beginning of the propagation because they are time independent. Likewise, the product $\mathbf{U} = \exp(-\mathbf{V}^{absorb}\Delta t/2)\,\mathbf{W}^{T}$ is formed once at the beginning of the propagation. The only time-dependent factor is $\exp(iE(t + \Delta t/2)\mathbf{d}\Delta t)$; this exponential can be calculated easily because $\mathbf{d}$ is a diagonal matrix. The cost for a propagation step for a linearly polarized pulse is proportional to $N_{\text{states}}{}^2$ and involves two full matrix-vector multiplies ($\mathbf{U}$ and $\mathbf{U}^T$) and three diagonal matrix-vector multiplies [$\exp(-i\mathbf{H}_{el}\Delta t/2)$ twice and $\exp(iE(t + \Delta t/2)\mathbf{d}\Delta t)$ once]. Because the propagation uses the exponential of the Hamiltonian, a fairly large time step of $\Delta t = 0.05$ a.u. (1.2 as) can be used. In similar simulations,[26] reducing the time step by a factor of 2 changed the ionization yield by less than 0.01%.

The corresponding Trotter factorization for a circularly polarized pulse involves two oscillating fields,

$$\begin{aligned}\mathbf{c}(t+\Delta t) &= \exp(-i\,\mathbf{H}_{el}\Delta t/2)\exp(-\mathbf{V}^{absorb}\Delta t/2)\\ &\quad\times \mathbf{W}_2^{T}\exp(i\,E_2(t+\Delta t/2)\,\mathbf{d}_2\,\Delta t/2)\,\mathbf{W}_2\\ &\quad\times \mathbf{W}_1^{T}\exp(i\,E_1(t+\Delta t/2)\,\mathbf{d}_1\,\Delta t)\,\mathbf{W}_1\\ &\quad\times \mathbf{W}_2^{T}\exp(i\,E_2(t+\Delta t/2)\,\mathbf{d}_2\,\Delta t/2)\,\mathbf{W}_2\\ &\quad\times \exp(-\mathbf{V}^{absorb}\Delta t/2)\exp(-i\,\mathbf{H}_{el}\Delta t/2)\mathbf{c}(t),\end{aligned} \tag{19}$$

where $\mathbf{W}_1\mathbf{D}_1\mathbf{W}_1{}^T = \mathbf{d}_1$ and $\mathbf{W}_2\mathbf{D}_2\mathbf{W}_2{}^T = \mathbf{d}_2$ are the eigenvalues and eigenvectors of the transition dipole matrices $\mathbf{D}_1$ and $\mathbf{D}_2$ in the two orthogonal field directions. A propagation step for a circularly polarized pulse involves four full matrix-vector multiplies and five diagonal matrix-vector multiplies.

A locally modified version of the Gaussian software package[29] was used to calculate the integrals needed for the TDCI simulations. Bond lengths for HBr and HI were 1.4484 and 1.6200 Å. The molecules were aligned with the z axis with the halogen in the +z direction. The calculation of HBr used the aug-cc-pVTZ basis set,[30–32] and calculations of HI used the aug-cc-pVTZ-PP basis set for I with a pseudopotential to account for relativistic effects in the core.[33] For the simulations of strong field ionization, these basis sets were augmented with an additional absorbing basis set consisting of diffuse functions placed on each atom (four *s* functions with exponents of 0.0256, 0.0128, 0.0064, and 0.0032; four *p* functions with exponents of 0.0256, 0.0128, 0.0064, and 0.0032; five *d* functions with exponents of 0.0512, 0.0256, 0.0128, 0.0064, and 0.0032; and two *f* functions with exponents 0.0256 and 0.0128)[17,26] for adequate interaction with the CAP. Calculations that included spin–orbit coupling used an effective one-electron spin–orbit operator that depends on Z_{eff}. The values for *Zeff* (1.00 for H, 35.2944 for Br, and 2416 for I) were optimized for these basis sets in our previous study.[24] The time-dependent wavefunctions included all excitations from the two highest σ orbitals and two highest π orbitals to all virtual orbitals with orbital energies less than 3 hartree. A total of 6608 and 8408 configurations were used to simulate the ionization of HBr^+ without spin–orbit coupling and HI^+ with spin–orbit coupling, respectively. The TDCI simulations were carried out with an external Fortran 95 code.

III. RESULTS AND DISCUSSION

Figure 2 shows the results for HBr ionized by a five cycle linearly polarized $\sin^2$ 800 nm pulse. The simulation starts with neutral HBr ($|\Psi_{neutral}|^2 = 1$) and the polarization direction of the field aligned parallel and perpendicular to the molecular axis. The field strength, $E_{\max} = 0.175$ a.u., is chosen to deplete the population of the neutral before the middle of the pulse and to produce a substantial amount of double ionization. The fraction of the neutral population that is ionized during each time step of the simulation is transferred to the cation. The population of the cation, $\langle\Psi_{cation}|\Psi_{cation}\rangle$, initially increases and then decreases as it is ionized to the dication ($\mathbf{V}^{\text{absorb}}\Psi_{cation} = \Psi_{dication}$). By the end of the pulse, the population of the neutral is zero and the sum of the populations of the cation

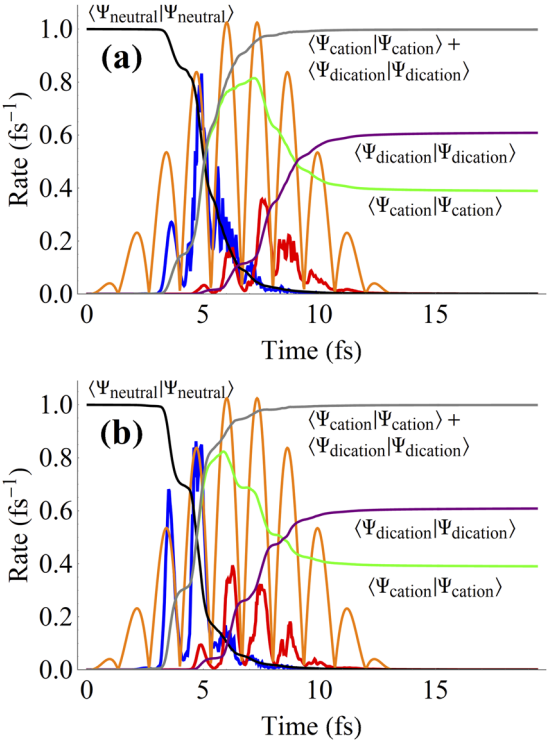

FIG. 2. Sequential double ionization of HBr (no spin–orbit coupling) by an intense, linearly polarized five cycle 800 nm $\sin^2$ pulse (E_{max} = 0.175 a.u.) with the polarization directions aligned (a) parallel and (b) perpendicular to the molecular axis: blue—ionization rate for the neutral, red—ionization rate for the cation, black—$\langle\Psi_{neutral}|\Psi_{neutral}\rangle$, green—$\langle\Psi_{cation}|\Psi_{cation}\rangle$, purple—$\langle\Psi_{dication}|\Psi_{dication}\rangle$, and gray—$\langle\Psi_{cation}|\Psi_{cation}\rangle + \langle\Psi_{dication}|\Psi_{dication}\rangle$; six times the absolute value of the electric field is shown in orange.

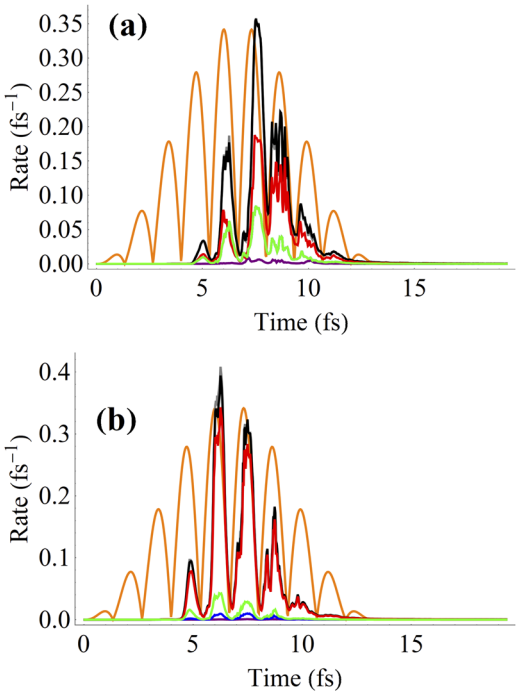

FIG. 3. Contributions to the total ionization rate of HBr^+ shown in Fig. 2 obtained from singular value decomposition of the absorbed wavefunction of the neutral for the polarization direction aligned (a) parallel and (b) perpendicular to the molecular axis (black—total; red, green, blue, and purple—SVD components with α and β contributions summed); the gray curve (almost totally hidden behind the black curve) is the total ionization rate of HBr^+ obtained from the partitioning of the total ionization rate into orbital contributions [Eq. (7)]; two times the absolute value of the electric field is shown in orange.

and the dication is one. The results are nearly identical if the cation populations are obtained by partitioning the ionization rate of the neutral into contributions from individual occupied orbitals [Eq. (7), shown in Fig. 2] or by singular value decomposition of the absorbed wavefunction, Eqs. (10)–(12).

In the sequential double ionization simulations, the TD-CIS simulations for the neutral yield an absorbed wavefunction that is taken as the wavefunction for the cation, $\mathbf{V}^{absorb}\Psi_{neutral} = \Psi_{cation}$. The wavefunction for the cation is a superposition of ground and excited states of the cation. Singular value decomposition can be used to partition the absorbed wavefunction into a set of components of the cation wavefunction [Eqs. (10)–(12)]. Since the cation wavefunction is an incoherent superposition of these components, a separate TD-CISD-IP simulation needs to be carried out for each component. The total rate of formation for the dication is then obtained by summing the individual contributions multiplied by $|w_K|^2$, the square of the SVD weights. Figure 3 shows the total rate of formation of the dication and the contributions from the different components of the cation wavefunction. For parallel alignment of the polarization direction with the molecular axis, the dominant component is ionization from the σ-type lone pair orbital; for perpendicular alignment, the dominant component is the π-type lone pair orbital. In both cases, the other orbitals contribute much less. Because the singular value decomposition is dominated by one contribution, the total rate of formation of the cation using Eqs. (10)–(12) (Fig. 3, black curve) is essentially the same as obtained

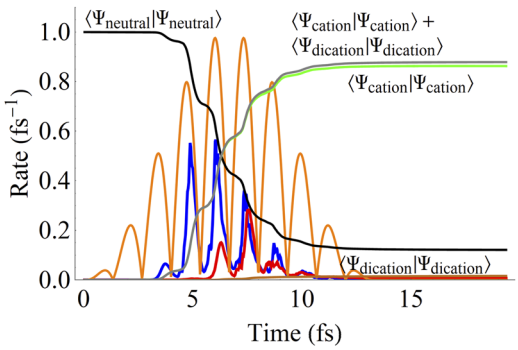

FIG. 4. Sequential double ionization of HBr (no spin–orbit coupling) by a less intense, linearly polarized five cycle 800 nm $\sin^2$ pulse (E_{max} = 0.10 a.u.) with the polarization direction aligned perpendicular to the molecular axis: blue—ionization rate for the neutral, red—50 times the ionization rate for the cation, black—$\langle\Psi_{neutral}|\Psi_{neutral}\rangle$, green—$\langle\Psi_{cation}|\Psi_{cation}\rangle$, purple—$\langle\Psi_{dication}|\Psi_{dication}\rangle$, and gray—$\langle\Psi_{cation}|\Psi_{cation}\rangle + \langle\Psi_{dication}|\Psi_{dication}\rangle$; 10 times the absolute value of the electric field is shown in orange.

from the partitioning of the total ionization rate into orbital contributions [Eq. (7), Fig. 3 gray curve, mostly hidden behind the black curve].

Experimental studies are more typically carried out with lower intensities such that the rate of formation of the dication is two orders of magnitude lower than the rate of formation of the cation. When the simulation in Fig. 2 is run with E_{max} = 0.10 a.u., the rate of formation of the dication is ~1/50 of the rate of formation of the cation, as shown in Fig. 4.

A casual inspection of neutral and cation ionization rates in Figs. 2 and 4 might suggest that there is a half cycle delay between the ionization of the neutral and the cation. However, the rate of formation of the dication depends on both the amount of cation formed in the first ionization and the rate of ionization for the cation, which in turn depends on the magnitude of the electric field. A much larger field is needed to ionize the cation because the ionization potential for the cation is much higher than for the neutral. Figure 5(a) shows a simulation for the ionization of HBr cation starting 5/8 of the way through the second cycle of the pulse. Ionization to the dication is seen as soon as the field reaches a maximum, but only about 15% of the cation is ionized in the half cycle. The next half cycle ionizes an additional 30% because the peak field strength is higher. This pattern is similar to the ones seen in Figs. 2 and 4, indicating that much of the variation in the cation ionization rate is due to the field strength rather than due to a delay between the first and second ionization. The variation in the peak field strength can be circumvented by using a continuous oscillating field in the simulation, as shown in Fig. 5(b). Most of the neutral HBr is ionized in the first half cycle. However, the field is not strong enough to ionize all of the cation within the first half cycle. More of the dication is produced in each of the subsequent half cycles. The rise time in the population of the dication compared to the rise time for the cation is dependent on the field strength and is not a good indicator of the time delay between the first and second ionization.

Simulations for the sequential double ionization of HI by an intense circularly polarized pulse are shown in Fig. 6. The wavefunction for HI includes spin–orbit coupling. The electric field for the pulse rotates in the xz plane, and the carrier envelope phase is chosen so that the maximum in the electric field is either parallel or perpendicular to the molecular axis. The ionization rate is seen to depend strongly on the carrier envelope phase, but this can be readily understood by looking at the details of the ionization. Ionization of HI is dominated by the p_π orbitals; peaks in the ionization rate occur at or

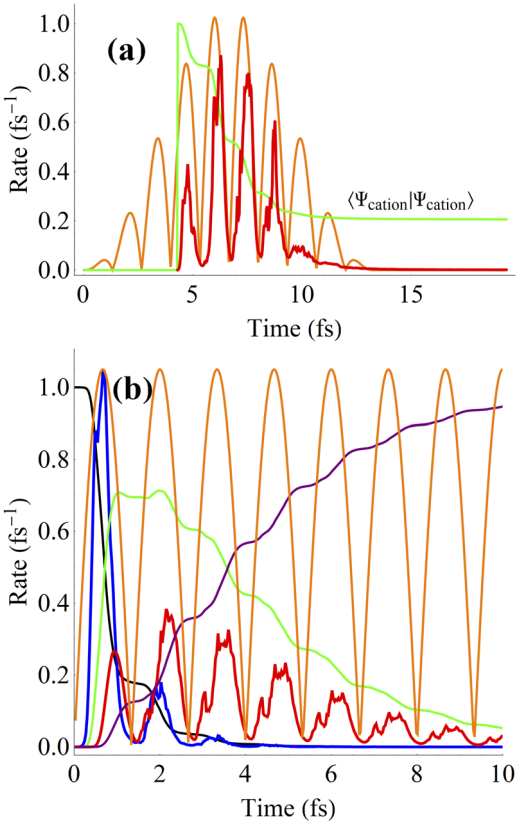

FIG. 5. (a) Ionization of HBr cation (red) starting 5/8 of the way through the second cycle of the pulse for the simulation described in Fig. 2(b); six times the absolute value of the electric field is shown in orange. (b) Ionization of HBr neutral (blue) and cation (red) by a CW 800 nm laser field; black—$\langle\Psi_{neutral}|\Psi_{neutral}\rangle$, green—$\langle\Psi_{cation}|\Psi_{cation}\rangle$, and purple—$\langle\Psi_{dication}|\Psi_{dication}\rangle$; five times the absolute value of the electric field is shown in orange.

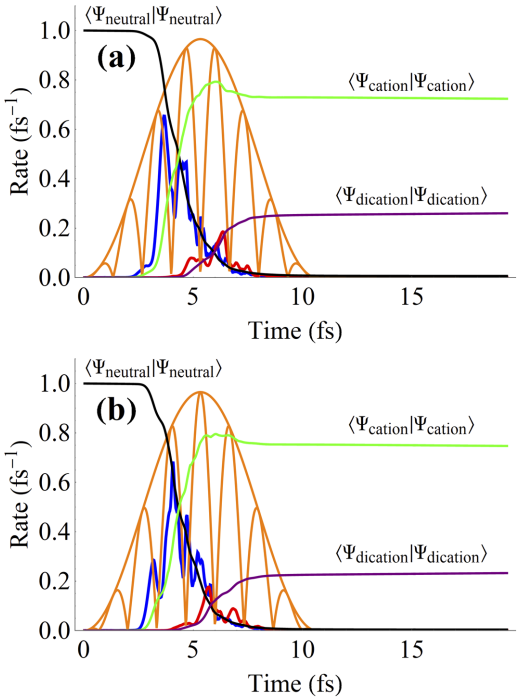

FIG. 6. Sequential double ionization of HI (with spin–orbit coupling) by an intense, circularly polarized four cycle 800 nm sin^2 pulse (E_{max} = 0.13 a.u.) with the electric field rotating in the xz plane with the maximum in the field (a) parallel and (b) perpendicular to the molecular axis: blue—ionization rate for the neutral, red—ionization rate for the cation, black—$\langle\Psi_{neutral}|\Psi_{neutral}\rangle$, green—$\langle\Psi_{cation}|\Psi_{cation}\rangle$, and purple—$\langle\Psi_{dication}|\Psi_{dication}\rangle$; 7.5 times the total field and 7.5 times the absolute value of the x component of the field are shown in orange.

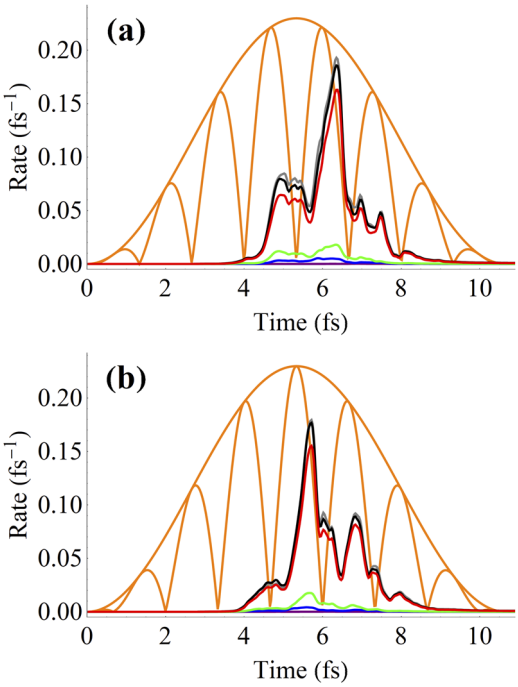

FIG. 7. Contributions to the total ionization rate of HI^+ shown in Fig. 6 obtained from singular value decomposition [Eqs. (10)–(12)] of the absorbed wavefunction of the neutral with the polarization direction aligned (a) parallel and (b) perpendicular to the molecular axis (black—total; red, green, blue, and purple—SVD components with α and β contributions summed); the gray curve (almost totally hidden behind the black curve) is the total ionization rate of HI^+ obtained with Eq. (7); 2.5 times the total field and 2.5 times the absolute value of the field perpendicular to the molecular axis are shown in orange.

shortly after the peaks in $|E_x|$, the x component for the electric field, i.e., when the field is aligned with the p_π orbital and depends on the height of the peak in $|E_x|$.

The singular value decompositions for the ionization of HI by a circularly polarized pulse are shown in Fig. 7. Similar to HBr, the ionization is dominated by one component of the cation wavefunction [the population method, Eq. (7), and the SVD method give essentially the same results for the total ionization yield]. The peaks in the rate of ionization of the cation to the dication occur at or shortly after the peaks in $|E_x|$, when the field is aligned with the p_π orbital.

IV. SUMMARY

A new method has been developed to simulate the strong field sequential double ionization process in molecular systems. The method fully incorporates both the amplitude and phase of the cation states produced by the first ionization and thus provides observations that can be compared with experimental results directly. The time-dependent ionization of the neutral is simulated with a TD-CIS calculation. At each time step, the ionized part of the wavefunction is transferred to a TD-CISD-IP calculation for ionization of the cation to the dication. This transfer is coherent and phase matched; it is achieved by decomposition of the first ionization rate into contributions from individual orbitals or by singular value decomposition of the absorbed wavefunction. This approach to sequential double ionization has been demonstrated for HBr in a five cycle 800 nm linearly polarized pulse and HI (with spin–orbit coupling) in a four cycle 800 nm circularly polarized pulse. The pulse intensities were chosen so that the population of the neutral was depleted by the mid-pulse. For the two orientations considered, the singular value decomposition shows that the cation produced by the first ionization is dominated by a single SVD component. Because the ionization potential for the cation is much higher than for the neutral, several cycles are needed to ionize a fraction of the cation population to the dication. The rise time for the dication population depends on the rise of the cation population and on the field intensity in the current and subsequent half cycles of the pulse rather than the ionization delay time. For HI with circularly polarized light, the rates for both the first and second ionization peak when the electric field is aligned with the p_π orbital.

ACKNOWLEDGMENTS

This work was supported by a grant from the National Science Foundation (Grant No. CHE1856437). We thank Wayne State University's computing grid for computer time.

DATA AVAILABILITY

The data that support the findings of this study are available from the corresponding author upon reasonable request.

REFERENCES

[1] D. N. Fittinghoff *et al.*, "Observation of nonsequential double ionization of helium with optical tunneling," Phys. Rev. Lett. **69**, 2642 (1992).
[2] T. Weber *et al.*, "Correlated electron emission in multiphoton double ionization," Nature **405**, 658 (2000).
[3] W. Becker *et al.*, "Theories of photoelectron correlation in laser-driven multiple atomic ionization," Rev. Mod. Phys. **84**, 1011 (2012).
[4] D. N. Fittinghoff *et al.*, "Polarization dependence of tunneling ionization of helium and neon by 120-fs pulses at 614 nm," Phys. Rev. A **49**, 2174 (1994).
[5] M. F. Kling *et al.*, "Control of electron localization in molecular dissociation," Science **312**, 246 (2006).
[6] A. H. Winney *et al.*, "Attosecond electron correlation dynamics in double ionization of benzene probed with two-electron angular streaking," Phys. Rev. Lett. **119**, 123201 (2017).
[7] A. Fleischer *et al.*, "Probing angular correlations in sequential double ionization," Phys. Rev. Lett. **107**, 113003 (2011).
[8] Y. Malakar *et al.*, "Time-resolved imaging of bound and dissociating nuclear wave packets in strong-field ionized iodomethane," Phys. Chem. Chem. Phys. **21**, 14090 (2019).
[9] A. N. Pfeiffer *et al.*, "Timing the release in sequential double ionization," Nat. Phys. **7**, 428 (2011).
[10] A. N. Pfeiffer *et al.*, "Breakdown of the independent electron approximation in sequential double ionization," New J. Phys. **13**, 093008 (2011).
[11] Y. Kobayashi *et al.*, "Coherent electronic-vibrational dynamics in deuterium bromide probed via attosecond transient-absorption spectroscopy," Phys. Rev. A **101**, 063414 (2020).
[12] J. H. Posthumus, "The dynamics of small molecules in intense laser fields," Rep. Prog. Phys. **67**, 623 (2004).
[13] K. L. Ishikawa and T. Sato, "A review on *ab initio* approaches for multielectron dynamics," IEEE J. Sel. Top. Quantum Electron. **21**, 8700916 (2015).

[14]M. Nisoli *et al.*, "Attosecond electron dynamics in molecules," Chem. Rev. **117**, 10760 (2017).
[15]J. J. Goings, P. J. Lestrange, and X. S. Li, "Real-time time-dependent electronic structure theory," Wiley Interdiscip. Rev.: Comput. Mol. Sci. **8**, e1341 (2018).
[16]A. Palacios and F. Martin, "The quantum chemistry of attosecond molecular science," Wiley Interdiscip. Rev.: Comput. Mol. Sci. **10**, e1430 (2020).
[17]P. Krause, J. A. Sonk, and H. B. Schlegel, "Strong field ionization rates simulated with time-dependent configuration interaction and an absorbing potential," J. Chem. Phys. **140**, 174113 (2014).
[18]M. K. Lee, W. Li, and H. B. Schlegel, "Angular dependence of strong field sequential double ionization for neon and acetylene simulated with time-dependent configuration interaction using CIS and CISD-IP," J. Chem. Phys. **152**, 064106 (2020).
[19]A. A. Golubeva, P. A. Pieniazek, and A. I. Krylov, "A new electronic structure method for doublet states: Configuration interaction in the space of ionized 1*h* and 2*h*1*p* determinants," J. Chem. Phys. **130**, 124113 (2009).
[20]C. M. Marian, "Spin-orbit coupling and intersystem crossing in molecules," Wiley Interdiscip. Rev.: Comput. Mol. Sci. **2**, 187 (2012).
[21]P. Krause and H. B. Schlegel, "Angle-dependent ionization of small molecules by time-dependent configuration interaction and an absorbing potential," J. Phys. Chem. Lett. **6**, 2140 (2015).
[22]P. Krause and H. B. Schlegel, "Angle-dependent ionization of hydrides AH_n calculated by time-dependent configuration interaction with an absorbing potential," J. Phys. Chem. A **119**, 10212 (2015).
[23]A. H. Winney *et al.*, "Disentangling strong-field multielectron dynamics with angular streaking," J. Phys. Chem. Lett. **9**, 2539 (2018).
[24]M. K. Lee *et al.*, "Effect of spin-orbit coupling on strong field ionization simulated with time-dependent configuration interaction," J. Chem. Phys. **153**, 244109 (2020).
[25]P. Hoerner and H. B. Schlegel, "Angular dependence of ionization by circularly polarized light calculated with time-dependent configuration interaction with an absorbing potential," J. Phys. Chem. A **121**, 1336 (2017).
[26]P. Hoerner and H. B. Schlegel, "Angular dependence of strong field ionization of CH_3X (X = F, Cl, Br, or I) using time-dependent configuration interaction with an absorbing potential," J. Phys. Chem. A **121**, 5940 (2017).
[27]P. Hoerner and H. B. Schlegel, "Angular dependence of strong field ionization of haloacetylenes, HCCX (X = F, Cl, Br, I) using time-dependent configuration interaction with an absorbing potential," J. Phys. Chem. C **122**, 13751 (2018).
[28]P. Hoerner, W. Li, and H. B. Schlegel, "Angular dependence of strong field ionization of 2-phenylethyl-*N*,*N*-dimethylamine (PENNA) using time-dependent configuration interaction with an absorbing potential," J. Phys. Chem. A **124**, 4777 (2020).
[29]M. J. Frisch *et al.*, Gaussian Development Version, Revision I.09, Wallingford, CT, 2010.
[30]T. H. Dunning, "Gaussian-basis sets for use in correlated molecular calculations. I. The atoms boron through neon and hydrogen," J. Chem. Phys. **90**, 1007 (1989).
[31]D. E. Woon and T. H. Dunning, Jr., "Gaussian basis sets for use in correlated molecular calculations. III. The atoms aluminum through argon," J. Chem. Phys. **98**, 1358 (1993).
[32]K. A. Peterson *et al.*, "On the spectroscopic and thermochemical properties of ClO, BrO, IO, and their anions," J. Phys. Chem. A **110**, 13877 (2006).
[33]K. A. Peterson *et al.*, "Systematically convergent basis sets with relativistic pseudopotentials. II. Small-core pseudopotentials and correlation consistent basis sets for the post-*d* group 16–18 elements," J. Chem. Phys. **119**, 11113 (2003).